Indian Journal of Chemistry
Vol. 57A, April 2018, pp. 469-476

Hydrogen bonded supramolecular architecture of a copper(II)-citrate coordination building block: Synthesis and crystal structure with theoretical insight

Sougata Sarkar[a,*], Dibakar Deb[b,*], Avijit Sarkar[c,*],
Shouvik Chattopadhyay[d,*], Bipan Dutta[e] & Soumen Khanra[a]

[a]Department of Chemistry, Ramakrishna Mission Vivekananda Centenary College, Rahara, Kolkata 700 118, India
Email: sougata.sarkar81@gmail.com

[b]Department of Chemistry, Techno India, Agartala 799 004, India
Email: debdibakar@gmail.com

[c]Department of Chemistry, Bhairab Ganguly College, Kolkata 700 056, India
Email: rite2avijit@gmail.com

[d]Department of Chemistry (Inorganic Section) Jadavpur University, Kolkata 700 032, India
Email: shouvik.chem@gmail.com

[e]Department of Physics, Sammilani Mahavidyalaya, Kolkata 700 094, India
Email: bipan.dutta@yahoo.com

A tricarboxylate supported binuclear metal organic hybrid of Cu(II), $[Cu_2(\mu\text{-cit})(phen)_4]\cdot 9H_2O$ (**1**) has been synthesized using the well known pyridyl based *N*,*N*′ linker, 1,10-phenanthroline and structurally characterized. The use of the flexible hydroxyl tricarboxylate citrate, in designing such a framework has created a marked diversity in the topology. The structural and topological diversity has been analyzed from the single crystal X-ray structure. Here, in a unit, each of the two Cu(II) centres is chelated by two phenanthroline ligands and citrate (cit^{4-}) serves the role of a bridging ligand. Furthermore, the carboxylate moiety/hydroxyl oxygen sites of citrate and the aromatic chelating ligands promote supramolecular recognition through hydrogen bonding and other non-covalent interactions (like π-π interaction) and water of crystallization, thereby resulting in a higher dimensional architecture. The oxygen atoms of the carboxylate moiety involve in both inter and intra-molecular hydrogen bonding with the water molecules resulting in a hydrogen bonded helical supramolecular solid. Theoretical study is performed to analyze the structure and the role of non-covalent interactions through DFT based calculations and Hirshfeld surface analysis.

Keywords: Supramolecular architectures, Density functional calculations, Crystal structure, Hydrogen bonding, π-π interactions, Copper, Citrate,

Crystal engineering of coordination polymers has attracted great attention in recent years due to their potential as functional materials as well as their interesting compositions and topologies[1]. These hybrid inorganic/organic materials with extended frameworks are thus worth mentioning owing to their interesting structures and potential applications in sorption, gas storage, enantio-separation, catalysis, sensing and magnetism[2]. Detailed mechanistic study suggests that these intriguing functionalities may have originated either from the organic portion and/or from the metal centers of the coordination moiety or might be a collective contribution from both the organic and inorganic members[3]. Since the last decade, the synthesis of metal carboxylates has grown exponentially due to the development of a new class of hybrid inorganic-organic materials with novel functionalities, which opened their scope of applications in the area of molecular adsorption, catalysis etc. These metal-organic frameworks (MOF) or coordination polymers have been constructed from the association of different types of metals together with different types of organic linkers[4]. Numerous coordination polymers have been prepared to date by the self-assembly of metal ions and multidentate ligands with various sizes and geometrical preferences. Many of these materials contain porous frameworks that mimic their inorganic counterparts, zeolites and molecular sieves, but with greater variety of sizes and shapes depending on the choice of building blocks. Although the general and precise principles for controlling the solid structures of the target products still need to be established, many rational synthetic strategies like hydrothermal,

solvothermal, reflux, etc. have been majorly highlighted and have proved to be significant in the way of fabrication of the metal-based coordination polymers[5]. Metal-carboxylato complexes have been of special interest because they not only form structurally interesting materials with fascinating properties but also act as single-source precursors for the preparations of high surface area multicomponent oxides materials (perovskites, spinels, ferrites, polytitanates, etc.)[6] among the possibilities of using aliphatic flexible poly-carboxylic acids/poly-carboxylates; malonate, succinate, fumarate, glutarate, adipate and their corresponding acids have been employed for the construction of a variety of coordination networks[7]. Attempts have also been made with hydroxyl poly-carboxylic acids/carboxylates, though comparatively not as much as that done before and in this connection, the use of tartaric acid/tartrates and citric acid/citrates are worth remembering[8,9]. Citric acid/citrate ion with its three carboxylic arms along with one hydroxyl group promotes the design of new metal cluster topologies by virtue of its coordinative flexibility and hence provides the opportunity to explore this commonly available laboratory chemical as a building block for the designing of hierarchical metal-organic coordination architectures. Here we have presented the synthesis of a Cu(II) based coordination polymeric system $[Cu_2(\mu\text{-cit})(phen)_4]\cdot 9H_2O$ (**1**), where a citrate-bound dimeric Cu(II) unit extends in space through hydrogen-bonded helical networks involving the lattice water molecules with the citrate backbone. DFT based calculation and Hirshfeld surface analysis is performed to analyze the stability and the role of non-covalent interactions contributing to the overall stability of complex **1** by focusing our attention to the hydrogen bonding interactions.

Materials and Methods

All the reagents were of analytical grade and used without further purification. All glassware were cleaned using aqua-regia, subsequently rinsed with copious amounts of double distilled water and dried well prior to use. Double distilled water was used throughout the course of the experiment**.**

Synthesis of the Complex $[Cu_2(\mu\text{-cit})(phen)_4].9H_2O$ (1)

A methanolic solution (10 mL) of 1,10-phenanthroline (0.18 g; 1 mmol) was added in a dropwise manner to an aqueous solution (5 mL) of copper(II) nitrate trihydrate (0.241 g; 1 mmol;) with stirring. After 30 min of stirring, an aqueous solution (5 mL) of trisodium citrate (0.258 g; 1 mmol) was poured slowly into the reaction mixture and stirring was continued. After stirring for 45 min, the deep-blue clear solution was refluxed for 3h, cooled and filtered. The clear blue filtrate was kept in a $CaCl_2$ desiccator. After 10 days, deep-blue block-shaped crystals, suitable for single crystal X-ray analysis were isolated from the medium. These were collected by filtration, washed with water and air dried. Yield: 0.028 g, 65%. Anal. Calc. for $C_{54}H_{54}Cu_2N_8O_{16}$ (1198.16 g mol^{-1}): Calculated: C, 54.13; H, 4.54; N, 9.35; Found: C, 54.10; H, 4.42; N, 9.26%. Selected FTIR bands: (KBr, cm^{-1}, vw = very weak, m = medium, s = strong, vs = very strong): 3512m ν(OH), 2830vw ν(CH), 2968vw ν(CH), 1611vs $\nu(OCO)_{asym}$, 1385s $\nu(OCO)_{sym}$, 2968m ν(C=N).

Physical Measurements

IR spectra were recorded with a Perkin Elmer Spectrum Spectrophotometer using KBr pellets in the region 4000–400 cm^{-1}.The single crystal X-ray diffraction data of all the compounds were collected on Apex Smart CCD system that uses graphite monochromated Mo-Kα radiation (λ = 0.71073 Å). The structure is solved by direct methods and refined by least square methods on F^2 employing WinGx[10] package and the relevant programs (SHELX-97[11] and ORTEP[12]) implemented therein. An empirical absorption correction is applied. Non-hydrogen atoms are refined anisotropically except the disordered oxygen atoms, which are refined isotropically.The hydrogen atoms connected to O-atoms of crystal water molecules cannot be located. The hydrogen atoms on C-atoms are fixed at calculated positions and refined using a riding model. Crystal structures are visualized and crystallographic numbering schemes are generated by the programs ORTEP[12], OLEX[13], MERCURY[14], DIAMOND[15]. All the calculations are carried out using PLATON[14] as incorporated in the WinGX suite[10]. The details of crystal data collection and refinement of the compound is summarized in Table 1. The important bond distances and bond angles are given in Table 2.

Hirshfeld Analysis

The Hirshfeld surfaces[16,17,18] and the associated 2D-fingerprint[19,20,21] plots were calculated using Crystal Explorer[22] which accepted a structure input file in CIF format. Bond lengths to hydrogen atoms were set to standard values. For each point on the

Table 1 — Crystallographic data, details of data collection and structure refinement parameters for $[Cu_2(\mu\text{-cit})(phen)_4].9H_2O$ (**1**)

Emp formula	$C_{54}H_{54}Cu_2N_8O_{16}$
FW (g/mol)	1198.16
T (K)	293(2)
Wavelength (Å)	0.71073
Crystal system	Monoclinic
Space group	P 2_1/n
a (Å)	11.9171 (5)
b (Å)	32.1152 (15)
c (Å)	15.9912 (7)
α (deg.)	90.00
β (deg.)	111.265 (2)
γ (deg.)	90.00
V (Å^3)	5703.4 (4)
Z	4
ρ_{calcd} (mg m^{-3})	1.373
μ (mm^{-1})	0.82
F(000)	2404
Crystal size (mm)	0.2×0.1×0.1
Measured reflections	83945
Unique reflections	14151
Observed reflections	10187
Parameters	740
R (int)	0.049
R_1 [I>2σ(I)], wR_2 (all reflns)[a]	0.0815, 0.2446
GOF on F^2	1.057
Largest diff. peak and hole (e.Å^{-3})	1.03 and -0.54

[a]Weighting scheme: $R_1=\Sigma(||F_o|-|F_c||)/\Sigma|F_o|$.
$wR_2 = [\Sigma w(|F_o|-|F_c|)^2/\Sigma w(F_o)^2]^{1/2}$.
Cal. $w = 1/(\sigma^2(F_o^2) + 0.0322P)^2 + 31.1256P$, where $P = (F_o^2+2F_c^2)/3$

Hirshfeld isosurface, two distances d_e, the distance from the point to the nearest nucleus external to the surface and d_i, the distance to the nearest nucleus internal to the surface, were defined. The normalized contact distance (d_{norm}) based on d_e and d_i was given by

$$d_{norm} = \frac{(d_i - r_i^{vdw})}{r_i^{vdw}} + \frac{(d_e - r_e^{vdw})}{r_e^{vdw}}$$

where r_i^{vdw} and r_e^{vdw} were the van der Waals radii of the atoms. The value of d_{norm} was negative or positive depending on intermolecular contacts, being shorter or longer than the van der Waals separations. The parameter d_{norm} displayed a surface with a red-white-blue colour scheme, where bright red spots highlighted shorter contacts, white areas represented contacts around the van der Waals separation, and blue regions were devoid of close contacts. For a given crystal structure and set of spherical atomic electron densities, the Hirshfeld surface was unique[23] and it was this property that suggested the possibility of gaining additional insight into the intermolecular interaction of molecular crystals.

Table 2 — Selected bond lengths and bond angles for complex (**1**)

Bond distances (Å)			
Cu1-O10	1.986(3)	Cu2-O8	1.992(3)
Cu1-N4	2.001(4)	Cu2-N5	2.002(4)
Cu1-N1	2.001(4)	Cu2-N7	2.007(4)
Cu1-N2	2.049(4)	Cu2-N6	2.058(4)
Cu1-N3	2.217(4)	Cu2-N8	2.211(4)
Bond angles (deg.)			
O10-Cu1-N4	91.92(15)	O8-Cu2-N5	91.74(14)
O10-Cu1-N1	91.71(15)	O8-Cu2-N7	95.55(14)
N4-Cu1-N1	176.27(16)	N5-Cu2-N7	171.52(15)
O10-Cu1-N2	159.50(16)	O8-Cu2-N6	156.94(15)
N4-Cu1-N2	95.43(19)	N5-Cu2-N6	81.75(15)
N1-Cu1-N2	81.44(19)	N7-Cu2-N6	93.09(15)
O10-Cu1-N3	97.45(15)	O8-Cu2-N8	102.49(15)
N4-Cu1-N3	79.35(16)	N5-Cu2-N8	95.46(15)
N2 Cu1 N3	102.71(16)	N7-Cu2-N8	78.76(16)
N1-Cu1-N3	99.32(17)	N6-Cu2-N8	100.15(14)

Computational Details

The theoretical calculations were done using Gaussion-09 suite of software[24]. Optimization of the metal complex was computed by Density Functional Theory (DFT). Becke's three parameter hybrid exchange (B3)[25], Lee-Yang-Parr correlation functional (LYP)[26]and 6-311++g(d,p) basis set were used for the DFT calculations. The natural bond orbital (NBO) analyses were carried out by considering the interactions between all the filled Lewis type (donor) $|\phi_i\rangle$ and unfilled non-Lewis (acceptor) $|\phi_j\rangle$ of the molecule. The interactions between their orbitals signify deviation of the molecule from the Lewis structure resulting from the electron delocalizations between the donor and the acceptor molecular orbitals. The electron delocalization lead to more stabilization of the molecule, whose degree is estimated from the stabilization energies $\Delta E_{ij}^{(2)}$, as obtained from second order perturbation theory. Accordingly,

$$\Delta E_{ij}^{(2)} = \frac{\left|\left\langle \phi_i \middle| F \middle| \phi_j \right\rangle\right|}{\varepsilon_i - \varepsilon_j}$$

where $\hat{F}$ is the Fock operator, ϵ_i and ϵ_j correspond to the energy eigen values of $|\phi_i\rangle$ and $|\phi_j\rangle$ molecular orbitals respectively.

Results and Discussion

Crystal structure of $[Cu_2(\mu\text{-cit})(phen)_4].9H_2O$

Blue colored single-crystals suitable for X-ray diffraction were obtained by slow evaporation of a saturated MeOH-H_2O solution of complex **1**. A perspective view of **1** with the atom-numbering scheme is shown in Fig. 1. Compound **1** crystallizes in the monoclinic system with $P2_1/n$ space group. The solved crystal structure of the complex contains two half asymmetric mononuclear copper (II) units which are equivalent and these two mononuclear units are in turn linked exclusively by one tri-carboxylato ligand coordinated by means of two of their carboxylate groups (Fig. 2) and nine water molecules as water of crystallization. Among the nine water molecules, four water molecules, O1W, O2W, O3W and O4W posses full occupancy. Four water molecules, O5W, O6W, O7W and O8W each possess half occupancy. In the molecule, three oxygen atoms, among the nine waters of crystallization, O9W, O10W and O11W are disordered. It is observed that O9W and O10W, each occupy two positions with half occupancy and O11W occupies three positions with occupancy 0.4, 0.4 and 0.2. The copper(II) ions in this complex are penta-coordinated in N_4O coordination environments and the corresponding τ values are 0.28 (Cu1) and 0.25 (Cu2), which clearly indicates that both the copper ions are in square pyramidal (SP) environment with a ~28% and ~25% trigonal-bipyramidal (*tbp*) distortion respectively (Fig. 3)[27]. Coordination environment around both the Cu(II) centers are composed of four nitrogen atoms of the chelating 1,10 phenanthroline (phen) ligand and one monodentate O-bonded citrate (cit^{4-}) anion. The basal plane of Cu1 is built up by four imine nitrogen atoms from phen [Cu1–N1 = 2.001(4), Cu1–N2 = 2.049(4) and Cu1–N4 = 2.001(4) Å] and carboxylate oxygen atom from one deprotonated anionic citrate ligand [Cu1–O10 = 1.986(3) Å][28].The axial position is occupied by one imine nitrogen atom from the phen ligand [Cu1–N3 = 2.217(4) Å]. Similarly the basal plane of Cu2 is formed by four imine nitrogen atoms [Cu2–N5 = 2.002(4), Cu2–N6 = 2.058(4) and Cu2–N7 = 2.007(4)] and one oxygen atom from citrate ligand [Cu2–O8 = 1.992(3) Å]. The coordination of Cu2 is completed by one apical copper-nitrogen atom distance [Cu2–N8 = 2.211(4) Å] from phen ligand. The *cis* angles around the Cu1, range from 79.35 to 102.71° with an average value of 92.42° and those around the Cu2 range from 78.76 to 102.94° with an average value of 92.37°. The two *trans* angles around

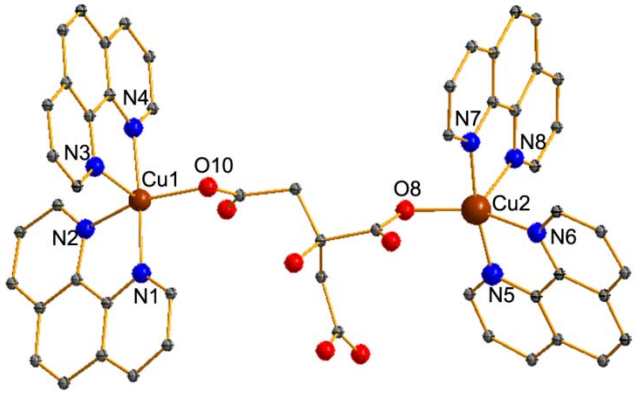

Fig. 1 — Molecular view of **1** with atom-numbering scheme. [H atoms are omitted for clarity. Color code: Cu(II) brown, N blue, O red, C gray].

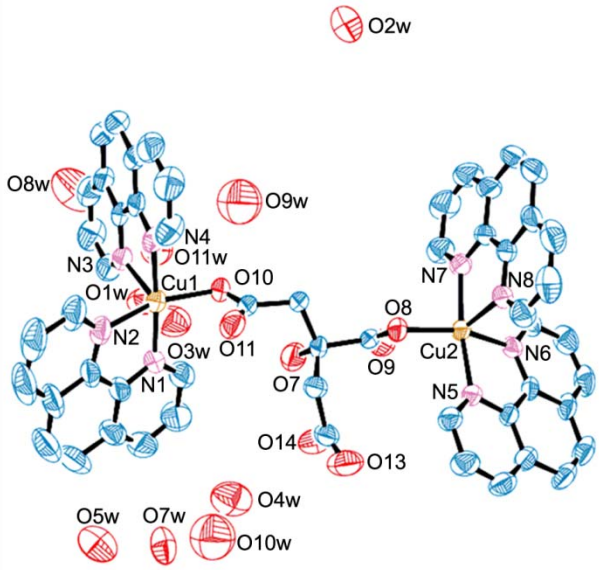

Fig. 2 — ORTEP view of the asymmetric unit of compound 6 with 30% thermal ellipsoid probability. Carbon atoms are not labelled and the hydrogen atoms are not shown in the figure and only a part of disordered molecules are shown for clarity.

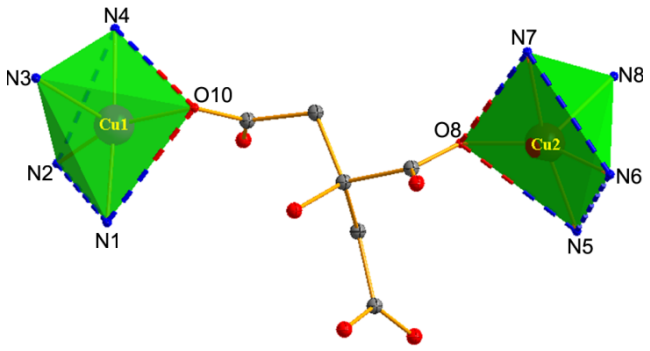

Fig. 3 — View of the atom connectivity and coordination geometry within [Cu2] unit in **1**.

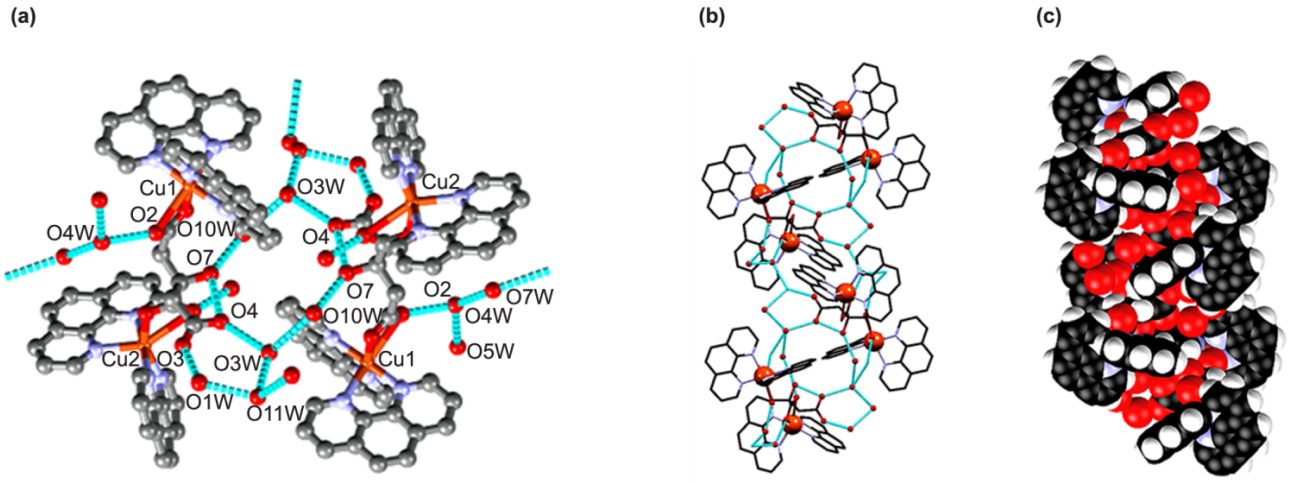

Fig. 4 — (a) Ball and stick model showing the coordination environment around copper centers and intra and inter molecular H-bonding interactions. [Colour code: Cu: Brick Red; O: red; N: light blue; C: black; H-bonding interactions: green dotted line. H-atoms are not shown for clarity]. (b) View of the H-bonded helical network extends along the crystallographic *c*-axis. (c) Spacefill model showing helical chain along the crystallographic *c*-axis. [Colour code: Cu: Brick Red; O: red; N: light blue; C: black; H-bonding interactions: sky-blue colour dotted line. H-atoms are not shown for clarity].

Cu1 are 176.27 and 159.50° and that around Cu2 are 171.52 and 156.94°.

In the crystal lattice, the molecule has hydrogen bond donor as well as acceptor sites and in the solid state it shows both intra and intermolecular hydrogen bonding interactions. We observe the hydrogen bonding interactions between carboxylate oxygen and water of crystallization as well as within crystal water molecules asO2-O4W, O4W-O5W, O5W-O5, O4W-O7W, O7W-O2W, O7W-O8W, O2W-O1W, O1W-O3, O11-O3W, O3W-O10W, O10W-O7, O3W-O4. The alcoholic oxygen, O7 is also hydrogen bonded with O10W. It is very interesting to note that due to the presence of extensive hydrogen bonding interactions in the solid state and due to presence of screw axis (-*x*+1/2, *y*+1/2, -*z*+1/2), we observe hydrogen bonded helical network which extends along the crystallographic *c*-axis. Overall in the solid state the compound forms a 3D supramolecular helical network as shown in Figs 4(a-c).

There are four significant π···π stacking interactions present within the as-synthesized complex. The phenyl ring, [C(18)-C(19)-C(20)-C(21)-C(26)-C(27)], is involved in an inter-molecular π···π interaction with symmetry related (-*x*,1-*y*,-*z*) phenyl ring, [C(18)-C(19)-C(20)-C(21)-C(26)-C(27)]. The other phenyl ring, [C(60)-C(61)-C(62)-C(63)-C(68)-C(69)], is also involved in an inter-molecular π···π interaction with symmetry related (2-*x*,1-*y*,1-*z*) phenyl ring, [C(60)-C(61)-C(62)-C(63)-C(68)-C(69)]. The phenyl

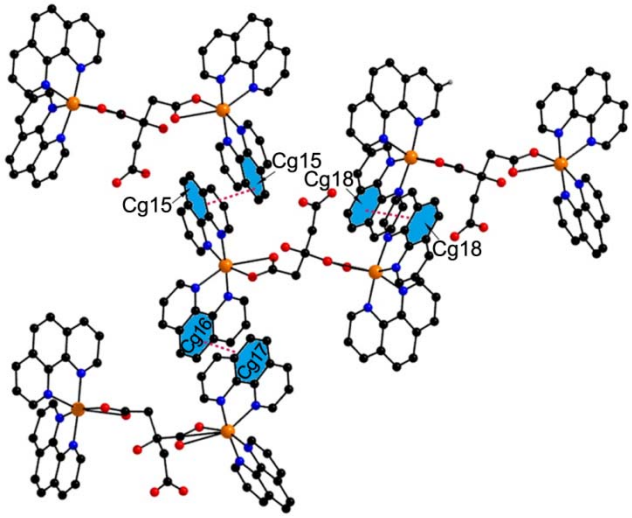

Fig. 5 — The π···π interactions in the complex (**1**). {Cg(15) = Centre of gravity of the ring [C(18)-C(19)-C(20)-C(21)-C(26)-C(27)], Cg(16) = Centre of gravity of the ring [C(32)-C(33)-C(34)-C(35)-C(40)-C(41)], Cg(17) = Centre of gravity of the ring [C(46)-C(47)-C(48)-C(49)-C(54)-C(55)], Cg(18) = Centre of gravity of the ring [C(60)-C(61)-C(62)-C(63)-C(68)-C(69)]}.

ring, [C(32)-C(33)-C(34)-C(35)-C(40)-C(41)], is stacked with symmetry related (-1/2+x,3/2-y,-1/2-z) phenyl ring, [C(46)-C(47)-C(48)-C(49)-C(54)-C(55)] (Fig. 5). The details of π···π interactions are given in Table 3.

Inter and intra molecular interactions

The Hirshfeld surfaces of the complex, mapped over d_{norm} (range of –0.1 to 1.5 Å), shape index and curvedness, are illustrated in Fig. 6. The surfaces are shown as transparent to allow visualization of the

molecular moiety around which they are calculated. The dominant interaction between O···H/H···O atoms can be seen in the Hirshfeld surfaces as red spots on the d_{norm} surface in Fig.6. Other visible spots in the Hirshfeld surfaces correspond to N···H contacts. The small extent of area and light colour on the surface indicates weaker and longer contact other than hydrogen bonds. The intermolecular interactions appear as distinct spikes in the 2D fingerprint plot (Fig. 7). Complementary regions are visible in the fingerprint plots where one molecule acts as donor (d_e<d_i) and the other as an acceptor (d_e>d_i). The fingerprint plots can be decomposed to highlight close contacts in certain atom pairs. This decomposition enables separation of contributions from different interaction types, which overlap in the full fingerprint. The proportions of O···H/H···O interactions comprise 15% of the Hirshfeld surfaces for the complex. This O···H/H···O interaction also appears as two distinct spikes in the 2D fingerprint plots (Fig. 7). The lower spike corresponding to the donor spike represents the O···H interactions (d_i = 1.4, d_e = 1.0 Å) and the upper spike being an acceptor spike represents the H···O interactions (d_i = 1.0, d_e = 1.4 Å) in the fingerprint plot (Fig. 7). Similarly the proportion of N···H/H···N interactions comprises 2.9% of the Hirshfeld surfaces for the complex. This N···H/H···N interaction also appears as two distinct spikes in the 2D fingerprint plots (Fig. 7). The lower spike corresponding to the donor spike represents the N···H interactions (d_i = 2.0,

Table 3 — Geometric features of the π···π interaction obtained for complex (**1**)

Cg(I)···Cg(J)[a]	Cg···Cg (Å)	Cg(I)···Per (Å)	Cg(J)···Per (Å)	α (◦)	β (◦)	γ (◦)	Symmetry
Cg(15)···Cg(15)	3.594(4)	3.493(3)	3.492(3)	0.0	13.65	13.65	*–x,*1*–y, –z*
Cg(18)···Cg(18)	3.522(6)	3.521(4)	3.522(4)	0.0	0.73	0.73	2*–x,*1*–y,*1*–z*
Cg(16)···Cg(17)	3.610(5)	3.408(4)	3.408(4)	1.6(4)	19.25	19.27	1/2+*x,*3/2*–y*, *–*1/2+*z*

[a]where, Cg(15) = Centre of gravity of the ring [C(18)-C(19)-C(20)-C(21)-C(26)-C(27)],
Cg(16) = Centre of gravity of the ring [C(32)-C(33)-C(34)-C(35)-C(40)-C(41)],
Cg(17) = Centre of gravity of the ring [C(46)-C(47)-C(48)-C(49)-C(54)-C(55)],
Cg(18) = Centre of gravity of the ring [C(60)-C(61)-C(62)-C(63)-C(68)-C(69)].

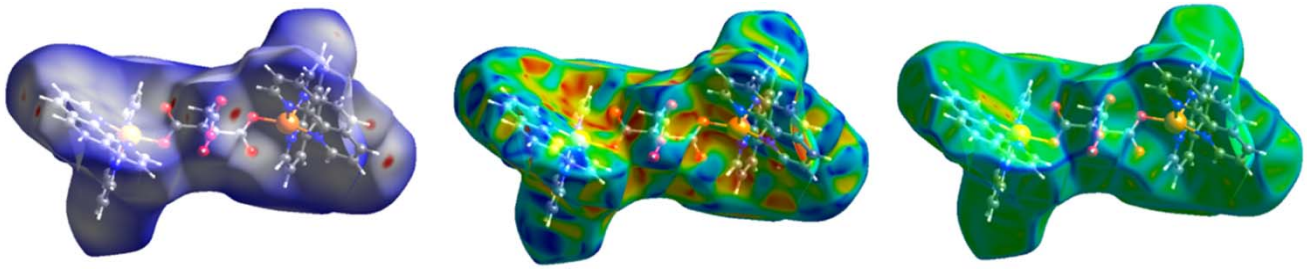

Fig. 6 — Hirshfeld surfaces mapped with d_{norm} (left), shape index (middle) and curvedness (right) of the complex.

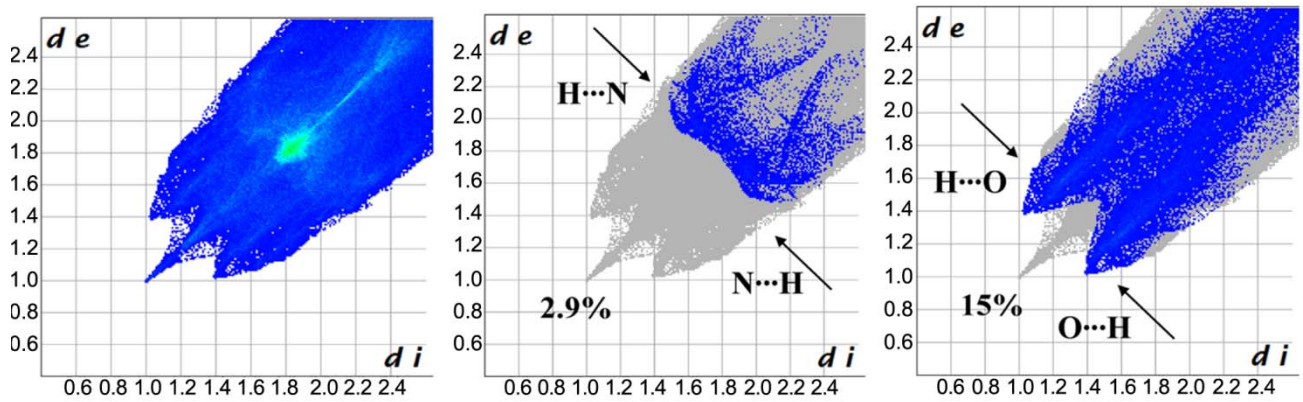

Fig. 7 — Fingerprint plot. {Full (left), resolved into H···N/N···H (middle), H···O/ O···H (right) contacts contributed to the total Hirshfeld surface area of the complex}.

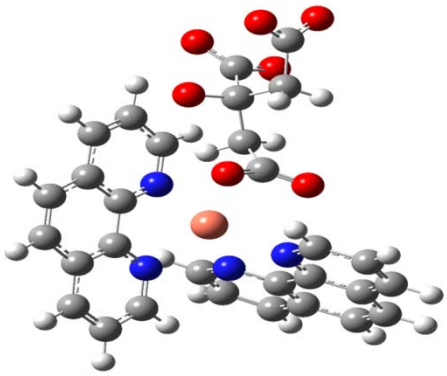

Fig. 8 — Optimized molecular geometry of **1**.

d_e = 1.5 Å) and the upper spike being an acceptor spike represents the H···N interactions (d_i = 1.5, d_e = 2.0 Å) in the fingerprint plot (Fig. 7).

Geometry optimization and electronic structure

Figure. 8 shows the structure of the complex along with its SCF energy (–1077440.3 kcal/mol). The structure of the metal complex belongs to C_1 point group symmetry. The relevant structural parameter of the complex is shown in the Table S1 (Supplementary Data). From Table S1, it is seen that the bond lengths between the central Cu_1 with respect to the nearest neighbour oxygen (O_2) and nitrogen (N_3, N_4, N_5 and N_6) atoms are quite similar. The NBO analyses have been performed to understand the stabilization energies between the central copper (Cu_1) and oxygen (O_2), nitrogen (N_3, N_4, N_5 and N_6) atoms of the metal complex (Supplementary Data, Table S2). From Table S2, it is clearly seen that appreciable stabilization energies arise from Cu1-N3(σ)/LP5*(Cu1), LP2(O_2)/LP6*(Cu1), LP2(N_4)/LP5*(Cu1), LP2(N_5)/LP5*(Cu1) and LP2(N_6)/LP8*(Cu1) bonding- antibonding orbital interactions of the complex. Fig. S1 (Supplementary Data) shows the corresponding 2D contour plots of the above-mentioned orbitals which exhibit favorable overlap in the region of Cu_1……O_2, Cu_1……..N_3, Cu_1……..N_4, Cu_1……..N_5 and Cu_1……..N_6 atoms for the metal complex. The appreciable overlap integral may lead to the possible charge transfer interaction between the metal and the ligands.

Conclusions

Here we have reported the synthesis of a citrate (an aliphatic tricarboxylate) bridged dimeric metal-organic coordination complex of Cu(II) in presence of a well known chelating ligand, 1,10-phenanthroline which binds to the metal centres. The dimeric unit is involved in supramolecular interactions through the participation of the hydrogen bonding and other non-covalent interactions (like π-π interaction) and hence results in a higher dimensional architecture. The synthesized molecular skeleton also encapsulates water of crystallization which in turn is involved in hydrogen bonding with the carboxylate moiety of the citrate. Some theoretical study has also been executed to scrutinize the role of non-covalent interactions through DFT based calculations and Hirshfeld surface analysis.

Supplementary Data

CCDC deposition number 1560258 for (**1**) contains the supplementary crystallographic data for complex (**1**). The data can be obtained free of charge via http://www.ccdc.cam.ac.uk/conts/retrieving.html or from the CCDC, 12 Union Road, Cambridge CB21EZ, UK; Fax: + 44-1223-336033; Email: deposit@ccdc.cam.ac.uk. Other supplementary data associated with this article are available in the electronic form at http://www.niscair.res.in/jinfo/ijca/IJCA_57A(04) 469-476_SupplData.pdf.

References

1 (a) Foo M L, Matsuda R & Kitagawa S, *Chem Mater*, 26 (2014) 310 (and references there-in); (b) Robin A Y & Fromm K M, *Coord Chem Rev,* 250 (2006) 2127 (and references there-in).

2 (a) Silva P, Vilela S M F, Tomé J P C & Paz F A A, *Chem Soc Rev*, 44 (2015) 6774 (and references there-in); (b) Mahapatra P, Drew M G B & Ghosh A, *Cryst Growth Des*, 17 (2017) 6809; (c) Navarro-Sánchez J, Argente-García A I, Moliner-Martínez Y, Roca-Sanjuán D, Antypov D, Campíns-Falcó P, Rosseinsky M J & Marti-Gastaldo C, *J Am Chem Soc*, 139 (2017) 4294; (d) Maity D K, Dey A, Ghosh S, Halder A, Ray P P & Ghoshal D, *Inorg Chem*, 57 (2018) 251; (e) Halder A, Kandambeth S, Biswal B P, Kaur G, Roy N C, Addicoat M, Salunke J K, Banerjee S, Vanka K, Heine T, Verma S & Banerjee R, *Angew Chem*, 128 (2016) 7937; (f) Bhattacharya B, Halder A, Paul L, Chakrabarti S & Ghoshal D, *Chem Eur J*, 22 (2016) 1.

3 Civalleri B, Napoli F, Noël Y, Roetti C & Dovesi R, *CrystEngComm*, 8 (2006) 364.

4 (a) Schoedel A, Li M, Li D, O'Keffe M & Yaghi O M, *Chem Rev*, 116 (2016) 12466; (b) Barnett S A & Champness N R, *Chem Soc Rev*, 246 (2003) 145.

5 Stock N & Biswas S, *Chem Rev*, 112 (2012) 933.

6 Banger K, Jin M H C, Harris J D, Fanwick P E & Hepp A F, *Inorg Chem*, 42 (2003) 7713.

7 (a) Bhattacharya B, Saha D, Maity D K, Dey R & Ghoshal D, *CrystEngComm*, 16 (2014) 4783; (b) Mitra M, Manna P, Bauza A, Ballester P, Seth S K, Choudhury S R, Frontera A & Mukhopadhyay S, *J Phys Chem B*, 118 (2014) 14713.

8 (a) Thushari S, Cha J A K, Sung H H Y, Chui S S Y, Leung A L F, Yen Y F & Williams I D, *Chem Commun*, 44 (2005) 5515; (b) Silva G B, Menezes P H, Malvestiti I,

Falcão E H L, Alves S, Chojnacki J & Silva F F, *J Mol Struct*, 1155 (2018) 530.
9 (a) Liao J H, Cheng S H & Su C T, *Inorg Chem Commun*, 5 (2002) 761; (b) Tabatabaee M, Hoseini R M & Parvez M, *Synth React Inorg Met-Org Chem*, 44 (2014) 775.
10 Farrugia L J, *J Appl Crystallogr*, 32 (1999) 837.
11 Sheldrick G M, *Acta Crystallogr Sect A*, 64 (2008) 112.
12 Farrugia L J, *J Appl Crystallogr*, 30 (1997) 565.
13 Dolomanov O V, Blake A J, Champness N R & Schroeder M, *J Appl Crystallogr*, 36 (2003) 1283.
14 Spek A L, *Acta Crystallogr D*, 65 (2009) 148.
15 DIAMOND, Visual Crystal Structure Information System, version 3;1, *Crystal Impact*, Bonn, Germany, 2004.
16 Spackman M A & Jayatilaka D, *CrystEngComm*, 11 (2009) 19.
17 Hirshfeld F L, *Theor Chim Acta*, 44 (1977) 129.
18 Clausen H F, Chevallier M S, Spackman M A & Iversen B B, *New J Chem*, 34 (2010) 193.
19 Rohl A L, Moret M, Kaminsky W, Claborn K, McKinnon J J & Kahr B, *Cryst Growth Des*, 8 (2008) 4517.
20 Parkin A, Barr G, Dong W, Gilmore C J, Jayatilaka D, McKinnon J J, Spackman M A & Wilson C C, *CrystEngComm*, 9 (2007) 648.
21 Spackman M A & McKinnon J J, *CrystEngComm*, 4 (2002) 378.
22 Wolff S K, Grimwood D J, McKinnon J J, Jayatilaka D & Spackman M A, Crystal Explorer 2;0, http:// hirshfeldsurfacenet;blogspot;com, (2007).
23 McKinnon J J, Spackman, M A & Mitchell A S, *Acta Crystallogr, Sect B: Struct Crystallogr Cryst Chem*, 60 (2004) 627.
24 Frisch M J, Trucks G W, Schiegel H B, Scuseria G E, Robb M A, Cheeseman J R, Montgomery J, Vreven T, Kudin K N & Burant J C, Gaussian 09; Gaussian, Inc: Pittsburgh, PA, (2009).
25 Backe A D, *J Chem Phys*, 98 (1993) 5648.
26 Lee C, Yang W & Parr R G, *Phys Rev B*, 37 (1988) 785.
27 Addison A W, Rao T N, Reedijk J, Rijn, J V & Verschoor G C, *J Chem Soc Dalton Trans*,7 (1984) 1349.
28 Akhtar M N, AlDamen M A, Chen Y C, Sadakiyo M, Khan J & Tong M L, *Inorg Chem Commun*, 83 (2017) 49.